RSC Advances

ROYAL SOCIETY OF CHEMISTRY

www.rsc.org/advances

Journal Name

ARTICLE

Theoretical Studies of Heteroatom-Doping in TiO_2 to Enhance the Electron Injection in Dye-Sensitized Solar Cells

Received 00th January 20xx,
Accepted 00th January 20xx

DOI: 10.1039/x0xx00000x

www.rsc.org/

Li Hao, Fu-Quan Bai*, Chui-peng Kong, Shamsa Bibi and Hong-Xing Zhang*

The density functional calculations have been explored to analyze the structural, electronic and charge transfer properties of the doped TiO_2 substrate and catechol-TiO_2 interfaces for dye-sensitized solar cells. The results demonstrate that dopant W^{6+} moves the CB (conduction band) edge downward and introduces 5d-unoccupied orbitals located in the CB bottom of the TiO_2. On the other hand, dopant Zn^{2+} shifts the CB edge upward with an insertion of 3d-occupied orbitals into the VB (valence band). In catechol-TiO_2 systems, W^{6+} enlarges the energy difference between the LUMO of catechol and LUMO of TiO_2, which enlarges the driving force for electron injection in turn and results in an increased short circuit current (J_{sc}). Our modeling injection dynamics and quantitative bader analysis of the interfacial charge transfer have revealed that the catechol-TiO_2 doped with W^{6+} provides faster and more electron injection for dye sensitized solar cells (DSSCs). While the Zn^{2+} doped system exhibits lower electron efficiency due to the minimized energy difference between the catechol LUMO and TiO_2 CB.

1 Introduction

Titanium dioxide (TiO_2) as a functional material has attracted considerable attention in recent decades because of its comprehensive combination of optical, electrical properties and important applications in photovoltaics[1-4] and photocatalysis[5-8]. In fact, the photovoltaics and photocatalysis performance of TiO_2 depends on electronic structure, interfacial properties and charge transport efficiency which are mostly determined by the crystal structure[9]. Introducing doping metal and non-metal atoms in TiO_2 have been proven as an efficient technology to achieve a higher photoelectric conversion [10-13] and photocatalytic efficiency[14-17]. In particular, doped TiO_2 materials have been recognized as promising candidates due to their size-tunable band gap and easy syntheses for photovoltaics and photocatalysis.

In the last two decades, one of the greatest achievements for clean energy applications is the dye-sensitized solar cells (DSSCs)[18]. DSSCs have been considering as an attractive candidate due to their low cost and high efficiency. In DSSC devices, TiO_2 photoanode acts as the electron acceptor in the electron injection process, and also provides direct or tortuous path for electron transport in the electrical circuits[19]. Intensive researches indicate that the driving force for electron injection is generated from the energy difference between the excited states of the dye and the CB (conduction band) edge of TiO_2[20, 21]. For single organic molecule, the steady LUMO (Lowest Unoccupied Molecular Orbital) can approximately express the excited states of the dye[22-24].So tuning of CB edge downward with dopants can enlarge the driving force and results more efficient electron injection[25-27], which is the key factor for the short-circuit photocurrent density (Jsc) and incident photon-to-electron conversion efficiency (IPCE)[28]. Dopants also play an important role in affecting the the properties of electrical conductivity and surface adsorption of TiO_2[29-32]. Therefore, introduction of dopants in TiO_2 effects the electron injection, the electron transport in the TiO_2 electrode and interface recombination between the injected electron and the oxidized redox mediator, I_3^- ions[33].

In order to achieve high-efficiency DSSCs, various types of dopants have been used for the optimization of TiO_2. Many studies have shown that doping nonmetal anions at O sites (e.g. B[34, 35], C[36], N[37, 38], S[39], and I[40]) induced additional electronic states above the valence band (VB) upper edge and scarcely had effect on CB near the bottom edge[41-43]. On the other hand, doping transition metal ions at Ti sites (such as Fe^{2+}[44], Ce^{4+}[45], Zr^{4+}[46], V^{4+} or V^{5+}[47], Nb^{5+}[48], Ta^{5+}[49] and W^{6+}[22]) is also be an effective method to modify the electronic properties of TiO_2. In a TiO_2 system, donor and acceptor-type dopants play different roles in terms of geometry and electronic structure, which affect the device performance in turn. Both of donor and acceptor-type transition metal ions dopants are thought to be very important for DSSC and have been extensively studied. Tungsten doping, as a donor-type dopant, was first reported by Ko et al.[10]; then Wang and coworkers[22] found that the CB edge of TiO_2 shifts downward gradually with increasing the tungsten (W^{6+}) content. Additionally, as an acceptor-type dopant, Zn-doped[50] TiO_2 enhanced the charge transfer under low-intensity illumination. According to previous studies, there are numbers of researches have reported that the electron

[a] International Joint Research Laboratory of Nano-Micro Architecture Chemistry, Institute of Theoretical Chemistry, Jilin University, 130023 Changchun, China. E-mail: baifq@jlu.edu.cn(F.-Q. Bai), zhanghx@mail.jlu.edu.cn(H.-X. Zhang).

injection process can be influenced by different dopants. The detailed mechanism of these influences remains to be elucidated.

In this work, an acceptor (Zn) and a donor dopant (W) in TiO_2 are studied to obtain insight into the mechanism by diverse dopants which affect the electron injection. We have performed a systematic analysis to investigate their effects on geometry and electronic structure, such as CB levels, CB component, density of states, and charge transfer. We have plotted the quantitative bader analysis and injection dynamics to explore the charge transfer between catechol and the TiO_2 surface. The acceptor (Zn) and donor (W) dopant play different roles to control the electron injection process in DSSCs and the corresponding results should provide valuable guidelines for experimental works.

2 Computational Details and Modeling

It is well known that anatase nanoparticles appear higher photovoltaic and photocatalytic activities compared with other titania polymorphs[51-53]. TiO_2(101) surface dominates more than 94% of the external surface in anatase crystal[54] and anatase (101) is the most well-known model describing the TiO_2 substrate in DSSC[55-57]. To assess the effects of heteroatom-doped TiO_2 electrodes on DSSC device performance, a large anatase (101) surface was constructed with a 15 Å vacuum layer as shown in Fig 1((10.21 Å*11.33 Å, (TiO_2)24, 72 atoms). Plane wave DFT calculations on the slab are performed in the Vienna Ab initio Simulation Package (VASP) code[58-60], using the projector-augmented plane-wave (PAW) pseudopotentials[61, 62] and generalized gradient approximation (GGA) of PBE[63, 64]. The cutoff energy is set to 600 eV. Geometries are optimized till the energy and force converged within fair limits (1×10^{-4}eV and 1×10^{-3} eV/Å respectively). Density of states (DOS) and the calculated scanning tunneling microscopes (STM) are obtained based on the optimized geometry. The brillouin zone of the surface is sampled using an 8×8×1 Monkhorst-Pack special k-point mesh to obtain and understand qualitative features on the geometrical and electronic structures of TiO_2 electrode.

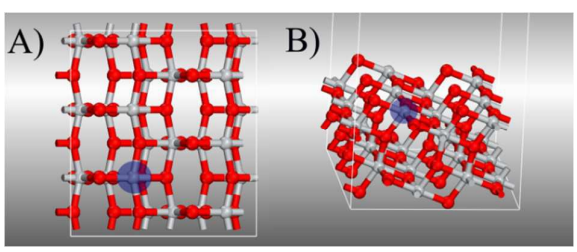

Fig.1 Supercell slab model of TiO_2 (101) surface. A) Top view B) Side view (Purple marked substituted Ti position)

Furthermore, a two-dimensional slab model of sensitized anatase (101) surface is built to describe the charge transfer between dye and the heteroatom-doped TiO_2 electrodes (The slab has dimensions of 10.21 Å*11.33 Å with a 20 Å vacuum layer). The same pseudopotential and function are utilized to calculate the electronic properties of dye/TiO_2 composite.

3 Results and discussion

3.1 Geometry and electronic properties of anatase(101)

As shown in Fig.1, heteroatom-doping of TiO_2 substrate has been implemented by substituting the surface 5-fold coordinated Ti (the purple position) with a W^{6+} or Zn^{2+} ion. The dopants in semiconductor oxides bring about serial changes in the geometrical and electronic structure. Based on the geometrical analysis, neither of W^{6+} and Zn^{2+} remains in the doped Ti site (Ti^{4+}) due to non-equilibrium charging. At the electron configuration of $3d^{10}$, Zn^{2+} changes the interatomic spacing and displays stretched distances with surrounding oxygen atoms. In addition, we have noticed that the Zn atoms try to move away from the surface position. In contrast, W^{6+} makes coordinate covalent bonds shorter than the corresponding Ti-O bonds because of the greater capacity to attract the electrons. As compared to doped Ti position of the pure TiO_2 electrode, W^{6+} and Zn^{2+} both move slightly along the [101] vector (z axis direction). The results demonstrate that z-coordinates are in the order of Zn^{2+} (7.15 Å) >Ti^{4+} (6.94 Å) >W^{6+} (6.88 Å) in the same coordinate system as shown in Fig.2.

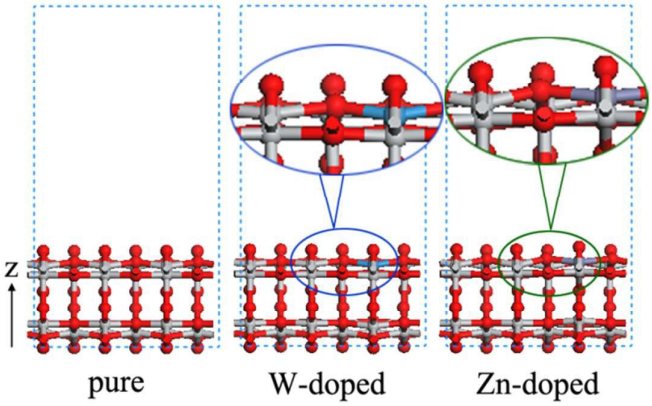

Fig.2 Structures of the pure and heteroatom-doped TiO_2 electrodes.

We have also investigated the effect of W^{6+} and Zn^{2+} doping on the electronic properties. The scanning tunneling microscopes (STM) images are generated based on the calculated charge density with a maximum z of 2.0 Å above the highest atom[65]. Contours added to STM images express the main features and different electronic structures of three TiO_2 super cells. For the STM images, F=− 1.40 V is used. The calculated STM images of filled states are illustrated in Fig 3 and some interesting features are also appeared in this image. The STM image of pure TiO_2 for a 1.4 V below the Fermi level provides a simple picture; light and shade are staggered periodically. In the panel d) of Fig.3, it is obviously shown that the egg-like shapes of the top layer are brighter than the second layer positions. There are distinct differences between

the doped semiconductor with W^{6+} and the pure TiO_2. The atom W located at second layer of the slab causes some interesting features in the STM image. A careful look at the panel e) reveals that darker and slightly smaller patterns of oxygen atoms surrounded the W^{6+} substituted site. However, the image still shows nicely pure TiO_2 features for the O atoms far from the W^{6+} site over three bonds. Taking a careful look on contour plots, it is can be seen that W^{6+} dopant reduced the charge density of the adjacent oxygen atoms. The STM image of Zn^{2+} doped TiO_2 shows the eye-catching bright ball of a top-layer O atom and dark gray oval shapes. The constant density surface, showed by the notch circle in the panel f), presents reduced charge density except the top O atom adjacent to Zn atom.

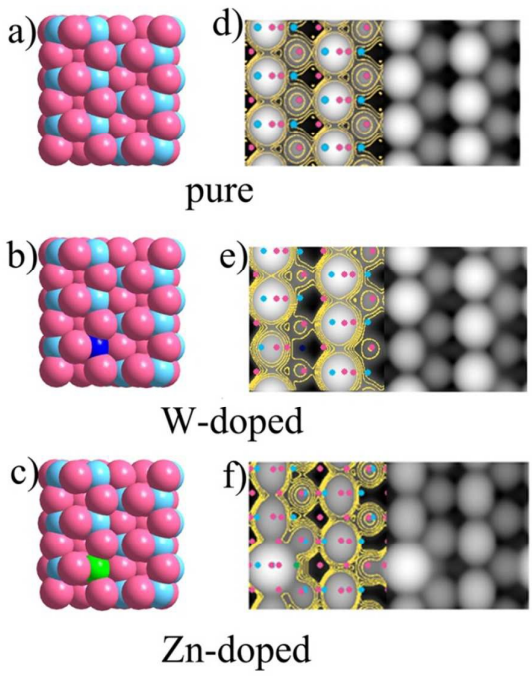

Fig.3 Atomic structures and calculated STM images of TiO_2(101) surfaces. Panels a) b) and c) represent the top views; d) e) and f) represent the STM images. Colored rounds label the atomic position: blue and fuchsia regions represent Ti and O atom positions in the two top layers of the surface, while cyan and green disks indicate the W and Zn atoms positions.

Furthermore, the DOS have been provided in Fig.4 for an indepth understanding of the interaction between W^{6+}/Zn^{2+} dopants and electronic properties. The DOS presents separated CB and VB, which are mainly composed of titanium 3d and oxygen 2p orbitals. Compared to the DOS of pure TiO_2, W^{6+} doping in TiO_2 moves the CB edge downward, which in turns enlarges the electron injection driving froce and increases the J_{sc}. Whereas, Zn^{2+} shiftes the CB and VB edge upward. The filled lines presented the d orbitals PDOS of W, Zn and corresponding site Ti atoms. It is worth noting that W^{6+} introduces some 5d-unoccupied orbitals located in the bottom of the TiO_2 CB, while dopant Zn^{2+}, with the configuration of $3d^{10}$, inserts 3d-occupied orbitals into the VB and the bottom edge of CB remains unchanged. In the ultrafast electron injection, excited electrons are injected into the TiO_2 CB; therefore, the CB component affects the electron injection distribution directly. Additionally, W^{6+} shifts the Fermi level negatively, which induces a better charge separation and would result in an enhancement of injection process.

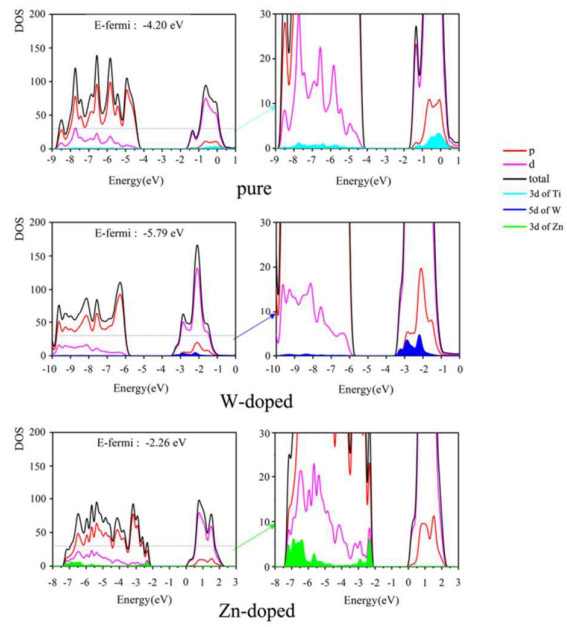

Fig.4 Calculated DOS (density of states) of TiO_2 (101) substrates. In the right panels, DOS have been zoomed in on. (The black line represents the total DOS; red and magenta lines represent the PDOS of titanium 3d and oxygen 2p orbitals; the filled cyan, green and blue lines represent the PDOS of W, Zn and corresponding site Ti d orbitals respectively in three slab models)

3.2 The effect of W^{6+}/Zn^{2+} dopants on the catechol-TiO_2 systems

3.2.1 The effect of W^{6+}/Zn^{2+} dopants on electronic structures of catechol-TiO_2 systems

Most researches have focused on the exploration of electron injection mechanisms by employing simple dye[19, 66-69]. Catechol ($C_6H_6O_2$) has been classified as representative examples of type-II dye, which follows a direct electron injection mechanism [19]. As catechol-TiO_2 interface can provide a clear and intuitive display of electron injection distribution, therefore, electronic structures of diverse catechol-TiO_2 were plotted out to analyze the effect of dopant W^{6+}/Zn^{2+} on the electron injection process.

The density of states are plotted to explore the interactions between catechol and the TiO_2. Compared to the bare TiO_2, the PDOS of TiO_2 adsorbed by catechol indicates a significant upward shift of the CB and VB edges. In Fig. 5, it can be clearly seen that there are strong overlap of the catechol with TiO_2. After adsorption, catechol introduces unoccupied molecular bands in the higher energy of conduction band. Zn^{2+} doped catechol-TiO_2 system shows a significantly overlap near the bottom edge of the conduction band, regarding PDOS of catechol. This minimizes the energy difference between the catechol LUMO and TiO_2 CB, which will induce a slower electron injection process compared with pure catechol-TiO_2

system. Wang and coworkers [22] have reported the open-circuit photovoltage (Voc) remained almost unchanged with less 0.5% W-doping due to the collective effect of the downward shift of the CB and the enhanced electron lifetime. As in Fig 5, W^{6+} shifts the PDOS of catechol away from the CB edge, which enlarges the energy difference between the catechol LUMO and TiO_2 CB. That would increase the driving force of electron injection and the Jsc in the DSSCs. The highest power conversion efficiency (η) was obtained in the experiments, with increasing by 17% in Jsc and by 20% in η[22].

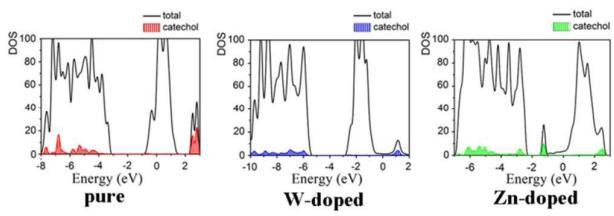

Fig. 5 Calculated DOS of catechol-TiO_2 systems (The black line represents the total DOS; the filled cyan, red and green lines represent the PDOS of catechol in W^{6+} doped, pure and Zn^{2+} doped slab models respectively).

The orbital distributions of valence band maximum (VBM) and conduction band minimum (CBM) at the Gamma point are illustrated in Fig. 6. The VBM maps are mostly localized on the catechol, which display diffusion to the adsorption sites at the catechol-TiO_2 interfaces. While the CBM are localized in the TiO_2 moiety, showing Ti-3d and W-5d orbitals characteristics; electron injection process will benefit. Moreover, the orbital distributions differ significantly in CBM as in panel d), the CBM distribution for pure catechol-TiO_2 mainly resides on the Ti 3d orbitals. With W^{6+} doping, as in panel e), the distribution of CBM concentrates in the region near the W^{6+} doping site of TiO_2. In panel f), Zn does not contribute any atomic orbitals to the CBM; the distribution of CBM mainly localized on the bottom layer of TiO_2 moiety. In the electron injection process, the TiO_2 electrode accepts electrons in conduction band from the excited dyes.It reveals that the effect of W^{6+}/Zn^{2+} dopants on CBM distributions of catechol-TiO_2 have significant impact on the electron injection process.

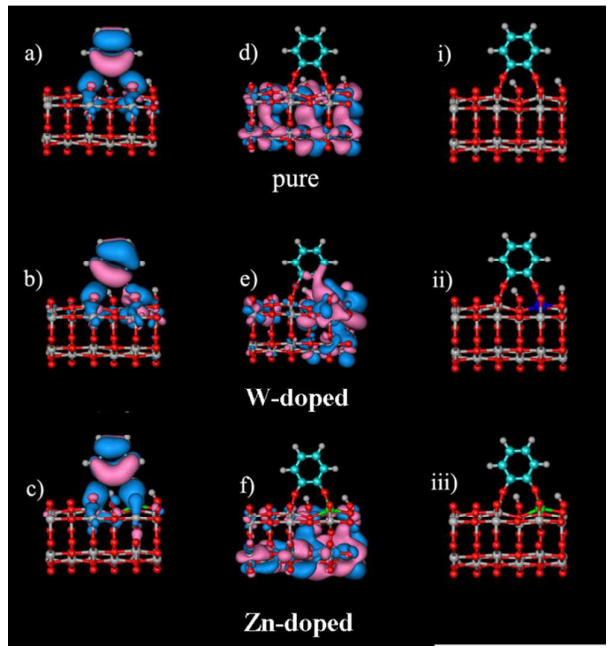

Fig. 6 Selected molecular orbitals of three catechol-TiO_2 systems. Left (panels a) b) and c)) and right (d) e) and f)) are the orbital distributions of the VBM and CBM for the Gamma point. i) ii) and iii) are the geometries of three catechol-TiO_2 systems.

3.2.2The effect of W^{6+}/Zn^{2+} dopants on electron injection through the catechol -TiO_2 interface

Dopants W^{6+} and Zn^{2+} differ the distributions and energy levels of CBM significantly, and influence the electron injection process and electron injection distribution further. Based on the bader charge analysis between catechol and TiO_2 electrodes, an increase in the TiO_2 electrodes charges is observed. In the pure catechol-TiO_2 system, there is 0.934*e* from the catechol fragment to TiO_2. In case of W^{6+} doping, 1.366*e* charge transfer into W^{6+} doped TiO_2 has been observed; conversely, Zn^{2+} doping decreaces the charge transfer with 0.443*e*. The diffrence in electronic density $\Delta\rho$ is presented in Fig. 7, which is estimated as follows:

$$\Delta\rho = \rho_{\text{total}} - \rho_{\text{catechol}} - \rho_{\text{TiO}_2}$$

Where ρ_{total} is the total electron density of catechol-TiO_2 system, $\rho_{catechol}$ and ρ_{TiO2} are the electron density of isolated catechol and TiO_2 fragment, respectively. As shown in Fig. 7, the fuchsia areas show where the electron density has been enriched; conversely, the blue regions show where the density has been depleted.

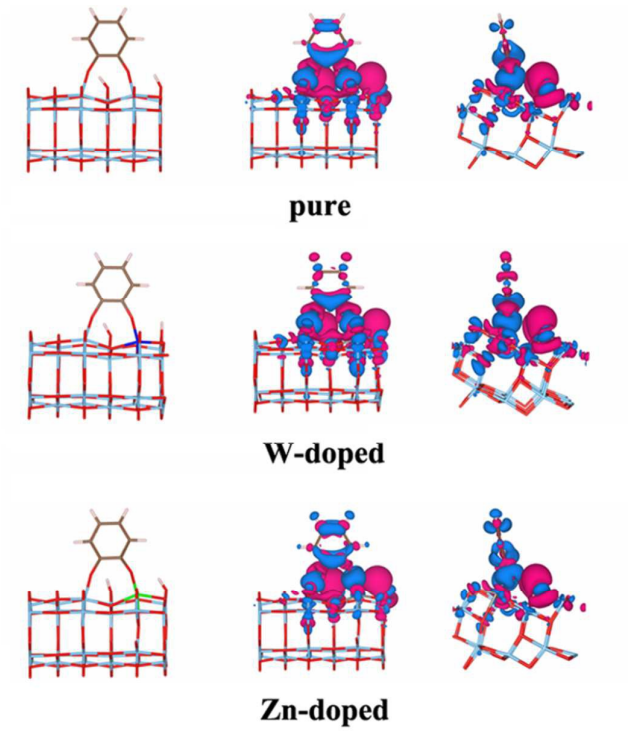

Fig. 7 The diffrence in electronic density between catechol and the TiO_2 (the fuchsia and blue areas refer to the increased and decreased electron density).

In addtion, dopants W^{6+} and Zn^{2+} also influence the dynamics of electron injection. The interfacical electron transfer has been simulated in the IET (Interfacial Electron Transfer) code [69, 70]; the further time-dependent survival probability in three different catechol sensitized TiO_2 are provided in Fig. 8. It exhibits fully consistent behavior with the staic charge transfer. Compared to pure catechol-TiO_2 system, W^{6+} doping provides faster and more electron injection, in addition to lower recombination. On the one hand doping W^{6+} resluts in a more efficient electron injection, but on the other hand it makes the back electron transfer easier. Conversely, Zn^{2+} doping exhibits a slower electron transfer and more incomplete electron injection.

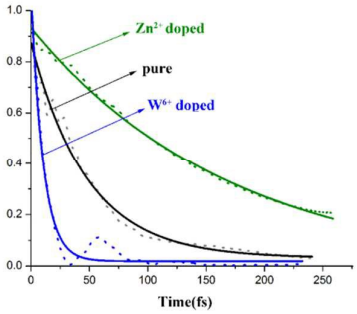

Fig. 8 The time-dependent survival probability in three different catechol sensitized TiO_2. The dashed lines correspond to elementary steps and the full lines are the exponential fitting. (Black, blue and green lines correspond to pure, W^{6+} and Zn^{2+} doped catechol-TiO_2 systems, respectively)

Conclusions

In this research, we report a theoretical investigation of heteroatom-doped TiO_2 electrode by modeling the TiO_2 photoanode and catechol-TiO_2 interface for DSSCs. The structural, electronic, and charge transfer properties of the catechol-TiO_2 interfaces have been considered for electron injection process. According to our study, the dopant W^{6+} may benefit the electron injection process by moving the CB edge downward and introducing 5d-unoccupied orbitals located in the CB bottom of the TiO_2. However, dopant Zn^{2+} shifts the CB edge upward with an insertion of 3d-occupied orbitals into the VB; while the bottom edge of CB remains unchanged. The quantitative analysis of charge transfer based on Bader analysis has exposed the critical electronic features underlying interfacial properties and interfacial electron transfers. The calculation reveals strong charge transfer between catechol and pure TiO_2 (0.934 *e*). W^{6+} has significantly increased the charge transfer toward the photoanode (1.366 *e*), while doping Zn^{2+} may cause the lowest charge transfer toward the adsorbate catechol with only 0.443 *e*. Furthermore, photo-induced charge transfer dynamics have also been described. It has indicated that the donor dopant W^{6+} accelerate the electron injection from dye to semiconductor, while the acceptor dopant Zn^{2+} slower the injection. Hence, it shows that diverse dopants can affect the electron injection process and provide valuable information. We thus envision that this theoretical investigation can provide important insights into the future design of more efficient materials for DSSCs.

Acknowledgements

This work was supported by the National Natural Science Foundation of China (Grant No. 21173096 and 21303068) and the State Key Development Program for Basic Research of China (Grant No.2013CB834801), and Young Scholar Training Program of Jilin University. The wavefunction plots are drawn with the help of the vaspmo program developed by Yang Wang. We also acknowledge Prof. Luis GC Rego for providing a copy of the IET code.

References

1 M. Gratzel, *Nature*, 2001, 414, 338-344.
2 M. Gratzel, Journal of Photochemistry and Photobiology C-Photochemistry Reviews, 2003, 4, 145-153.
3 A. Hagfeldt and M. Gratzel, *Accounts of Chemical Research*, 2000, 33, 269-277.
4 F. De Angelis, *Accounts of Chemical Research*, 2014, 47, 3349-3360.
5 A. Fujishima and K. Honda, *Nature*, 1972, 238, 37-38.
6 A. Fujishima, X. Zhang and D. A. Tryk, *Surface Science Reports*, 2008, 63, 515-582.
7 F. Zuo, K. Bozhilov, R. J. Dillon, L. Wang, P. Smith, X. Zhao, C. Bardeen and P. Feng, *Angewandte Chemie International Edition*, 2012, 51, 6223-6226.
8 J. Schneider, M. Matsuoka, M. Takeuchi, J. Zhang, Y. Horiuchi, M. Anpo and D. W. Bahnemann, *Chemical Reviews*, 2014, 114, 9919-9986.

9 G. Liu, H. G. Yang, J. Pan, Y. Q. Yang, G. Q. Lu and H.-M. Cheng, *Chemical Reviews*, 2014, 114, 9559-9612.
10 K. H. Ko, Y. C. Lee and Y. J. Jung, *Journal of Colloid and Interface Science*, 2005, 283, 482-487.
11 X. Lu, X. Mou, J. Wu, D. Zhang, L. Zhang, F. Huang, F. Xu and S. Huang, *Advanced Functional Materials*, 2010, 20, 509-515.
12 Y.-C. Nah, I. Paramasivam and P. Schmuki, *ChemPhysChem*, 2010, 11, 2698-2713.
13 K. Lee, A. Mazare and P. Schmuki, *Chemical Reviews*, 2014, 114, 9385-9454.
14 H. Irie, Y. Watanabe and K. Hashimoto, *Chemistry Letters*, 2003, 32, 772-773.
15 T. Ohno, T. Mitsui and M. Matsumura, *Chemistry Letters*, 2003, 32, 364-365.
16 S. In, A. Orlov, R. Berg, F. García, S. Pedrosa-Jimenez, M. S. Tikhov, D. S. Wright and R. M. Lambert, *Journal of the American Chemical Society*, 2007, 129, 13790-13791.
17 L. Sang, Y. Zhao and C. Burda, *Chemical Reviews*, 2014, 114, 9283-9318.
18 B. O'Regan and M. Gratzel, *Nature* 1991, 353, 737-740.
19 W. R. Duncan and O. V. Prezhdo, *Annual Review of Physical Chemistry*, 2007, 58, 143-184.
20 A. Hagfeldt, G. Boschloo, L. Sun, L. Kloo and H. Pettersson, *Chemical Reviews*, 2010, 110, 6595-6663.
21 D. Cahen, G. Hodes, M. Gratzel, J. F. Guillemoles and I. Riess, *The Journal of Physical Chemistry B*, 2000, 104, 2053-2059.
22 X. Zhang, F. Liu, Q.-L. Huang, G. Zhou and Z.-S. Wang, *The Journal of Physical Chemistry C*, 2011, 115, 12665-12671.
23 K.-P. Wang and H. Teng, *Physical Chemistry Chemical Physics*, 2009, 11, 9489.
24 X. Ren, Q. Feng, G. Zhou, C.-H. Huang and Z.-S. Wang, *The Journal of Physical Chemistry C*, 2010, 114, 7190-7195.
25 C. Klein, M. K. Nazeeruddin, P. Liska, D. Di Censo, N. Hirata, E. Palomares, J. R. Durrant and M. Gratzel, *Inorganic Chemistry*, 2005, 44, 178-180.
26 Z.-S. Wang, Y. Cui, Y. Dan-oh, C. Kasada, A. Shinpo and K. Hara, *The Journal of Physical Chemistry C*, 2008, 112, 17011-17017.
27 G. Zhou, N. Pschirer, J. C. Schöneboom, F. Eickemeyer, M. Baumgarten and K. Müllen, *Chemistry of Materials*, 2008, 20, 1808-1815.
28 M. Gratzel, Journal of Photochemistry and Photobiology C: Photochemistry Reviews, 2003, 4, 145-153.
29 K. Suriye, P. Praserthdam and B. Jongsomjit, *Applied Surface Science*, 2007, 253, 3849-3855.
30 F. Dong, S. Guo, H. Wang, X. Li and Z. Wu, *The Journal of Physical Chemistry C*, 2011, 115, 13285-13292.
31 A. Zaleska, *Recent Patents on Engineering*, 2008, 2, 157-164.
32 Z. Zhao, Z. Li and Z. Zou, *The Journal of Physical Chemistry C*, 2013, 117, 6172-6184.
33 A. J. Frank, N. Kopidakis and J. v. d. Lagemaat, *Coordination Chemistry Reviews*, 2004, 248, 1165-1179.
34 H. Tian, L. Hu, C. Zhang, S. Chen, J. Sheng, L. Mo, W. Liu and S. Dai, *Journal of Materials Chemistry*, 2011, 21, 863-868.
35 A. Subramanian and H.-W. Wang, *Applied Surface Science*, 2012, 258, 6479-6484.
36 R. Taziwa, E. L. Meyer, E. Sideras-Haddad, R. M. Erasmus, E. Manikandan and B. W. Mwakikunga, *International Journal of Photoenergy*, 2012, 2012, 904323(904321-904329).
37 T. Ma, M. Akiyama, E. Abe and I. Imai, *Nano Letters*, 2005, 5, 2543-2547.
38 M. Motlak, M. S. Akhtar, N. A. M. Barakat, A. M. Hamza, O. B. Yang and H. Y. Kim, *Electrochimica Acta*, 2014, 115, 493-498.
39 Q. Sun, J. Zhang, P. Wang, J. Zheng, X. Zhang, Y. Cui, J. Feng and Y. Zhu, *Journal of Renewable and Sustainable Energy*, 2012, 4.
40 Q. Hou, Y. Zheng, J.-F. Chen, W. Zhou, J. Deng and X. Tao, *Journal of Materials Chemistry*, 2011, 21, 3877-3883.
41 X. Chen, C. Burda, J. Guo, K. E. Smith, P.-A. Glans and T. Learmonth, *Arabian Journal for Science and Engineering*, 2010, 35, 65-71.
42 X. Chen, P.-A. Glans, X. Qiu, S. Dayal, W. D. Jennings, K. E. Smith, C. Burda and J. Guo, *Journal of Electron Spectroscopy and Related Phenomena*, 2008, 162, 67-73.
43 N. Serpone, *The Journal of Physical Chemistry B*, 2006, 110, 24287-24293.
44 L. Sang, J. L. Gole, J. Wang, J. Brauer, B. Mao, S. M. Prokes and C. Burda, *The Journal of Physical Chemistry C*, 2013, 117, 15287-15294.
45 J. Zhang, W. Peng, Z. Chen, H. Chen and L. Han, *The Journal of Physical Chemistry C*, 2012, 116, 19182-19190.
46 M. Durr, S. Rosselli, A. Yasuda and G. Nelles, *The Journal of Physical Chemistry B*, 2006, 110, 21899-21902.
47 K. Bhattacharyya, S. Varma, A. K. Tripathi, S. R. Bharadwaj and A. K. Tyagi, *The Journal of Physical Chemistry C*, 2008, 112, 19102-19112.
48 A. K. Chandiran, F. d. r. Sauvage, M. Casas-Cabanas, P. Comte, S. M. Zakeeruddin and M. Graetzel, *The Journal of Physical Chemistry C*, 2010, 114, 15849-15856.
49 J. Liu, H. Yang, W. Tan, X. Zhou and Y. Lin, *Electrochimica Acta*, 2010, 56, 396-400.
50 K.-P. Wang and H. Teng, *Physical Chemistry Chemical Physics*, 2009, 11, 9489-9496.
51 D. C. Hurum, A. G. Agrios, K. A. Gray, T. Rajh and M. C. Thurnauer, *The Journal of Physical Chemistry B*, 2003, 107, 4545-4549.
52 K. Woan, G. Pyrgiotakis and W. Sigmund, *Advanced Materials*, 2009, 21, 2233-2239.
53 B.-M. Kim, S.-G. Rho and C.-H. Kang, *Journal of Nanoscience and Nanotechnology*, 2011, 11, 1515-1517.
54 M. Lazzeri, A. Vittadini and A. Selloni, *Physical Review B*, 2001, 63, 155409.
55 L.-M. Liu, S.-C. Li, H. Cheng, U. Diebold and A. Selloni, *Journal of the American Chemical Society*, 2011, 133, 7816-7823.
56 F. Schiffmann, J. VandeVondele, J. Hutter, R. Wirz, A. Urakawa and A. Baiker, *The Journal of Physical Chemistry C*, 2010, 114, 8398-8404.
57 J. Yu, J. Fan and K. Lv, *Nanoscale*, 2010, 2, 2144-2149.
58 G. Kresse and J. Hafner, *Physical Review B*, 1993, 47, 558-561.
59 G. Kresse and J. Furthmüller, *Physical Review B*, 1996, 54, 11169-11186.
60 G. Kresse and J. Furthmuller, *Computational Materials Science*, 1996, 6, 15-50.
61 P. E. Blochl, *Physical Review B*, 1994, 50, 17953-17979.
62 G. Kresse and D. Joubert, *Physical Review B*, 1999, 59, 1758-1775.
63 J. P. Perdew, K. Burke and M. Ernzerhof, *Physical Review Letters*, 1996, 77, 3865-3868.
64 J. P. Perdew, K. Burke and M. Ernzerhof, *Physical Review Letters*, 1997, 78, 1396-1396.
65 D. E. P. Vanpoucke and G. Brocks, *Physical Review B*, 2008, 77, 241308.
66 L.-M. Liu, S.-C. Li, H. Cheng, U. Diebold and A. Selloni, *Journal of the American Chemical Society*, 2011, 133, 7816-7823.
67 R. Sanchez-de-Armas, M. A. San-Miguel, J. Oviedo and J. F. Sanz, *Computational and Theoretical Chemistry*, 2011, 975, 99-105.
68 R. o. Sanchez-de-Armas, J. Oviedo, M. A. n. San Miguel and J. F. Sanz, *The Journal of Physical Chemistry C*, 2011, 115, 11293–11301.
69 L. G. C. Rego and V. S. Batista, *Journal of the American Chemical Society*, 2003, 125, 7989-7997.
70 W. Li, L. G. C. Rego, F.-Q. Bai, J. Wang, R. Jia, L.-M. Xie and H.-X. Zhang, *The Journal of Physical Chemistry Letters*, 2014, 5, 3992-3999.